Viscoelastic properties of electrospray-deposited polymer shells via quartz crystal microbalance with dissipation (QCM-D)

Robert A. Green-Warren[1, §], Noah M. McAllister[1], Parameshwaran Pasupathy[1], Assimina A. Pelegri[1], Jonathan P. Singer[1], N. Sanjeeva Murthy[,2]*

[1]Department of Mechanical and Aerospace Engineering, Rutgers University, Piscataway, NJ, 08854, USA
[2]Laboratory for Biomaterials Research, Department of Chemistry and Chemical Biology, Rutgers University, Piscataway, NJ, 08854, USA

Keywords: Polymer shells, nanoparticles, thin films, electrospray deposition, viscoelasticity, quartz crystal microbalance with dissipation

Correspondence: N.Sanjeeva Murthy
Laboratory for Biomaterials Research, Department of Chemistry and Chemical Biology, Rutgers University, Piscataway, NJ, 08854, USA
E-mail: nsmurthy@chem.rutgers.edu

Abstract

Multilayer polymer films have found significant applicability to multiphase separation applications. The viscoelastic properties of polymer nanoshell coatings fabricated by electrospray deposition (ESD) were evaluated using Quartz Crystal Microbalance with Dissipation (QCM-D). Polymer coatings were deposited on gold-coated quartz crystals and spin-coated polystyrene (PS) surfaces. As the ESD flow rate increased from 0.5 to 1.5 mL/h, the thickness of PS films on gold increased from ~200 to 400 nm, with a corresponding order-of-magnitude increase in dissipation due to larger particle sizes from shorter droplet flight times. This effect was absent on spin-coated PS films, suggesting the onset of self-limiting effect of charges on the spin-coated PS substrate. Shear moduli for ESD coatings on gold were virtually independent of flow rate and consistent with expanded polystyrene foams. The QCM-D modulus of the spray-coated film was only 0.08-0.20% of the bulk PS modulus, yet the stiffness ratio of spray-coated PS to a single shell was (5.00 - 13.3) x 10^3 m^{-1}, attributed to rigid shell-shell and shell-substrate interactions. These are novel results related to the interparticle friction obtained using QCM-D's for the first time. Our work highlights the capability of QCM-D to predict mechanical properties of particulate viscoelastic films with nanogram quantities, demonstrating potential applications in high surface area sensors, such as size-selective membranes for protein or electrolyte adsorption.

1. Introduction

Porous polymer films are emerging as critical components of numerous engineering applications including gas separations, desalination, aerosol capture, and energy storage systems. Polymer films can be synthesized through various methods of polymer-solvent phase separation and are often categorized as supported or free-standing films. Supported films can be produced by drop casting, spin coating, and electrospray deposition (ESD), whereas free standing films are commonly generated through a process such as phase inversion.[1-4]

ESD is a technique notable for its ability to generate uniform polymer films with tunable morphologies.[5-8] Tunability, i.e., fine control of the microstructure, thickness, and porosity is achieved through manipulation of the electrospray parameters, such as input voltage, polymer-solvent concentration, separation distance, and solution conductivity.[5, 9] In the self-limiting electrospray deposition (SLED) regime, electrostatic charge build-up leads to the formation of conformal micron-scale porous coatings on 2D and 3D surfaces.[4, 6, 10] The ability of SLED to coat both conductive and non-conductive surfaces is highly advantageous for coating various materials, with past and current examples including, most commonly, metals and semiconductors, but also glass, hydrogels, living tissue, and gold plated quartz.[11-13] Additionally, SLED is capable of producing nanoscale and microscale particles, leading to desirable surface characteristics such as super hydrophobicity and hydrophilicity, resulting in films with tunable absorption and adsorption properties.[14, 15] These coatings are generally in the form of partially fused polymeric shells because of the evaporation kinetics of the solvent and the viscosity of PS; other morphologies, including nanowires, can also be generated.[4, 10] An illustration of the gold-plated QCM sensor after electrospray (ES) is shown in **Figure 1**. The coatings deposited in this work are sprayed in the SLED regime, but since the thickness is too small to trigger the self-limiting effect, it will be simply referred to as ESD films.

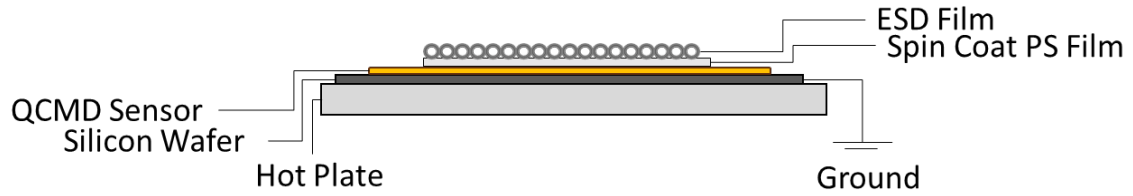

Figure 1. Schematic of the coated layers leading to a monolayer of PS particles atop a spin coated PS layer, and finally the quartz sensor. Silicon wafer is used as a ground and the hotplate can be used to adjust substrate temperature.

In our previously published report of the mechanical characterization of SLED films, we demonstrated the effects of film morphology on the quasistatic mechanical response of SLED films using various model polymers.[5] Nanoindentation with a conospherical tip was used to evaluate SLED film response to compressional loads at low strain-rates. Further, laser induced projectile impact test (LIPIT) is often utilized to evaluate a materials ability to dissipate the energy of high speed impact using ceramic or polymer based microprojectiles, 3-30 μm in diameter.[16] Ren et al. compared LIPIT and sphero-conical nanoindentation results from PS by evaluating volumetric energy dissipation.[17] They show that the primary source of dissipation during nanoindentation is due to the collapse of the hollow particles. In contrast, thermo-mechanical annealing and crazing were significant contributors to energy dissipation under high-speed impact, in the range of 200-900 m/s.[17] However, it was found that at depths greater than 50% of the original film thickness, substrate rigidity and particle confinement effects also contribute to the elastic behavior of SLED films under both loading conditions.[5, 17] Since both nanoindentation and LIPIT suffer from effects of confinement, film-substrate interactions, and loading configuration such as indenter tip size for nanoindentation and projectile size for LIPIT, alternative methods to evaluate the mechanical behavior of ESD films are necessary to fully characterize them across a wide spectrum of strain rates.

In this paper, we introduce quartz crystal microbalance with dissipation (QCM-D) to evaluate the morphology and mechanical properties of ESD films. QCM uses the mass

dependence of the resonance frequency (~ 5 MHz) of a piezoelectric quartz crystal to measure nanogram changes in mass by measuring frequency changes (Δf) with a precision of 1-2 Hz. In QCM-D, instead of continuous oscillation of the crystal, the crystal is pinged at millisecond intervals to observe the decay of these oscillations. The rate and magnitude of this decay is used to measure changes in dissipation (ΔD).[18] Because lower frequency oscillations propagate farther away from the surface than higher frequency ones, it is possible to capture the depth-dependence of the viscous properties of the layers deposited onto the gold surface by monitoring several harmonics. Such measurements and detailed analysis of multiple harmonics can be used to examine the mechanical response of ESD particles to shear stresses at megahertz frequencies.[19]

2. Results and Discussion

ESD films with particle sizes between 10^1-10^2 μm can be measured using optical microscopy. Since the particles of the ESD PS coatings are often too small to be resolved at visible wavelengths, they are typically evaluated using SEM.[20, 21] **Figure 2** is a top-down view of the various coatings studied in this work, obtained using SEM. Particle diameters in the range 1-5 μm, decorated with smaller secondary particles <1 μm, have been observed for the electrospray parameters used in this study.[5] The morphology of polymer shells is largely dictated by solution flow rate, solvent evaporation kinetics, and viscosity of the polymer-solvent blend.[4, 22] Particle diameters for 0.5 mL/h are ~ 1 μm compared to those sprayed at 1.5 mL/h, which have a nominal diameter between 3-5 μm (Figure 2). Morphologies of the porous PS films deposited via ESD onto bare gold surface (S1-S4) and onto spin-coated PS surface (S5-S8) were similar.

Figure 2. Top-down SEM images of the ESD coatings made with the following coating conditions (a) 0.5 mL/h PS on Au (b) 0.5 mL/h PS on Spin Coated PS (c) 0.5 mL/h on Spin Coated PS aged for 24 hrs under ambient conditions (d) 1.5 mL/h PS on Au (e) 1.5 mL/h on spin coated (f) Spin coat PS (g) 1.5 mL/h on spin coated PS after thermal annealing at 120ºC for 20 secs on a hotplate. All scale-bars are 1 μm.

QCM-D experiments consisted of measuring the Δf and ΔD data sequentially on bare sensors (S1-S8) as a benchmark, after spin coating one layer of PS (S5-S8), after spray coating (S1-S8), after ambient aging for ~24 hours (S1-S8), and finally, after thermal annealing (S1-S8). **Figure 3** is a representative plot of the Δf and ΔD shifts for S6, which was obtained by stitching each curve into one data frame. The plots for all other sensors can be found in **Figures S1 - S4**. The results for sensor S6 are summarized in **Table 1**.

2.1 Frequency and dissipation changes

The data in Figure 3 is a composite of five distinct sections corresponding to different coating conditions. While Δf, to a first approximation, represents the change in mass or thickness of an adsorbed layer, ΔD reflects the viscoelastic behavior of this layer. The decrease in Δf at ~1.8 h arises from the addition of the spin coat PS layer, whose Sauerbrey mass is ~14 μg. Negative

Figure 3. Raw frequency and dissipation data plot for sensor 6 (S6). The five data segments from separate measurements done on different days were "stitched" (see Experimental Section), and are presented as one continuous scan for visualization. The discontinuities in the data are artifacts of this stitching.

dissipation values are observed (Table 1) for the spin coated film. However, since these values are very small (ΔD ~2 x 10^{-6} -10^{-7} for Δf of 10^2 -10^3 Hz), they can be approximated to be zero.

These zero shifts in ΔD indicates that the films are rigid and strongly bound to the gold substrate. The similarities in Δf and ΔD values for sensors S5-S6 and S7-S8 (Table 1) is indicative of the uniform mass deposition of the spin coated PS film for these crystals. The second shift at ~3 h reflects the addition of the spray coated PS particles. The decrease in Δf corresponds to the additional spray deposited PS particles. The dramatic increase in ΔD is due to viscoelastic behavior of the assembly of PS shells and their interaction with the substrate; the dissipation arises primarily from the interparticle and particle-sensor interfaces.[23, 24] The third change in Δf induced at ~ 4-hour mark was caused by the removal of the sensor and reinserting it after

aging at ambient conditions for 24 h, to continue the data collection. The positive shift in frequency, and the associated gradual negative shift in dissipation, usually indicate significant change in or microstructure during aging.[19] In our case, it is most likely due to the evaporation of adsorbed/absorbed moisture in the porous ESD layer. Upon thermal annealing most of the porosity and the associated adsorbed moisture is eliminated. This give rise to the fifth and final change in Δf and ΔD. Here, Δf increases and ΔD returns to the initial value (~1.8 h mark) as the PS particles fuse into a smooth and rigid thin film free of porosity.

The two sets of gold substrates with spray coated films (S1, S2 and S3, S4, deposited at 0.5 and 1.5 ml/h for 18 and 6 minutes, respectively) contained same volume of solution, 0.15 ml. Interestingly, film thickness doubles from ~200 to ~400 nm when the flow rate increases from 0.5 to 1.5 ml/h, respectively. The dissipation increases by approximately a factor of 20 from ~40 in S1-S2 to ~700 x 10^{-6} in sensors S3-S4; the latter of which was sprayed at the higher flow rate. Indicating that ESD films fabricated at lower flow rates behavior more rigidly than those sprayed at higher flow rates.

Within the spin coated films (S5-S8), the dissipation is small (ΔD ~0). This indicates that the spin coated PS film rigidly adheres to the gold surface upon deposition and displays is indicative of elastic behavior. In this sense, the film is behaving as an extension of the thickness of the quartz sensor. Therefore, the Sauerbrey approximation (**Equation 1**) is used to obtain the thickness, *t*, of the spin-coated film, and is 120 -140 nm (Δf 740-900 Hz). **Figure 4** shows a plot of the Sauerbrey mass and thickness for S6 as a function of time, corresponding to the five stages in Figure 3. As described in the Experimental Section, Sauerbrey equation is valid for spin-coated and annealed films for which ΔD ~0. It is also valid for ESD samples at 0.5

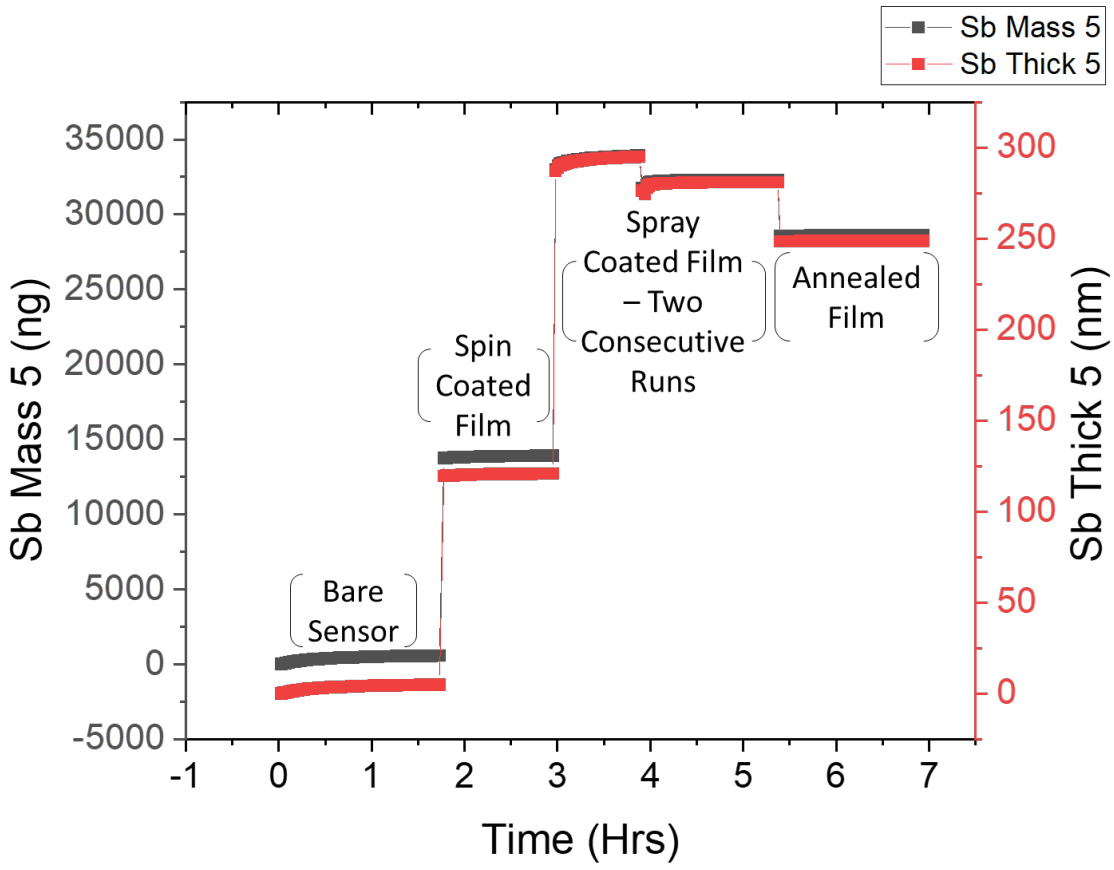

Figure 4. Plot of fitted Sauerbrey mass and Sauerbrey thickness vs. time, represented by the gray and red squares, respectively. The discontinuities in the data are artifacts of "stitching" in an attempt to present five separate data sets in one plot as in Figure 3.

ml/h, both before and after annealing, where $\Delta D < 0.3^{*}\ 10^{-6}$ per 10 Hz in Δf. Voigt model was necessary only for Sensors 3 and 4, and perhaps 8, and even in these samples, only for the step between 3 and 5 h with ESD particles at 1.5 ml/h and before annealing. In these instances, Voigt model was used to fit both the ESD PS shells on gold and on spin-coated PS. Even in these instances, because the $\Delta D/\Delta f$ are not too large, Voigt- and Sauerbrey-masses were not that different (Table I). Thus, to keep the plot simple, Sauerbrey masses was used for all the sensors and all time points in Figure 4.

The effective mass (i.e. areal density) determined via QCM-D for the ESD samples, calculations were compared with mass estimated from the mean particle size (1 and 5 μm for 0.5 and 1.5 mL/h, respectively; from SEM images) and mean shell wall thickness (estimated as 50 and 100 nm, respectively). By assuming a monolayer of PS particles, the theoretical areal density was determined to be 19 and 40 $\mu g/cm^2$ for 0.5 and 1.5 mL/h, respectively. These values are in good agreement with mass values obtained from QCM-D measurements (**Table 1)**.

2.2 Viscoelastic and Elastic Modelling

Data from the spray coated films in which the dissipation was appreciable ($> 1 \times 10^{-7}$ Hz^{-1}) were fit to the Voigt model of viscoelasticity.[25] The Voigt model, in which a spring and a dashpot are arranged in parallel, represents the behavior of an elastic solid undergoing viscoelastic strain. An alternative Maxwell model has a spring and a dashpot arranged in series. When this model is subjected to a stress, the spring deforms immediately while the dashpot deforms linearly with a constant strain-rate. Thus, the model does not predict creep accurately. With prolonged application of a small stress, the strain can become very large, resembling fluid-like behavior.[26] The Voigt shear modulus (G) in the table refers to the complex modulus at megahertz frequencies, consisting of both elastic and inelastic components.[27] G obtained via QCM-D is determined by the phase lag between the input and output signals, and is thus limited to films exhibiting viscoelastic behavior. For a stiff layer rigidly adhered to the sensor surface (no-slip condition at the film-sensor interface), dissipation is negligible.[28] Sauerbrey approximation is used to analyze these data. Therefore, there are no values for Voigt mass or shear moduli in Table 1 for the *Spin Coated Film* and *Thermally Annealed* Films sections. Dramatic decreases in dissipation, similar to that shown here for annealed films, have been observed in QCM-D studies evaluating the collapse of vesicles into lipid bilayers and formation of thin films from nanoparticles upon adsorption.[23, 24] The complex moduli of porous and non-

Table 1. Changes in frequency, dissipation and the calculated mass, thickness, shear modulus obtained for all the polystyrene films via QCMD. In the table, G is the shear modulus, t is effective film thickness, and ρ is the approximate density of bulk PS.

Sensors	1	2	3	4	5	6	7	8
Rate [mL/hr.]	0.5	0.5	1.5	1.5	0.5	0.5	1.5	1.5
Time [min]	18	18	6	6	18	18	6	6
Spin Coated Films*								
Δf [Hz] 5th harmonic	-	-	-	-	-775	-738	-895	-884
ΔD [10^{-6}]	-	-	-	-	0.25	-1.83	-0.23	-0.18
Sauerbrey Mass [μg-cm^{-2}]	-	-	-	-	14.3	14.3	15.6	16
Voigt Mass [μg-cm^{-2}]	-	-	-	-	-	-	-	-
t [nm] [r=1050 g/cc]	-	-	-	-	121	121	140	138
Shear Modulus G [MPa]	-	-	-	-	-	-	-	-
Spray Coated Films								
Δf [Hz] 5th harmonic	-1667	-1388	-2717	-2805	-872.4	-1839	-1040	-1187
ΔD [10^{-6}]	43.1	44.4	732	637	2.64	28.6	21.3	133
Sauerbrey Mass [μg-cm^{-2}]	30	25.5	52.5	52.5	16	34	19	22
Voigt Mass [μg-cm^{-2}]	23.5	20	52.5	47.5	15.4	30	19.3	26
t [nm] [r= 1050 g/cc]	260	220	416	433	137	295	165	190
Shear Modulus G [MPa]	2.85	2.03	2.34	2.30	-	5.25	2.15	1.08
Annealed Films								
Δf [Hz] 5th harmonic	-1330	-917.1	-2470	-2746	-833.8	-1633	-1089	-1396
ΔD [10^{-6}]	12.96	-16.4	71.3	105.7	2.59	9.42	8.76	42.35
Sauerbrey Mass [μg-cm^{-2}]	23.8	19.0	51.0	45.8	15.3	28.3	17.3	26.0
Voigt Mass [μg-cm^{-2}]	-	-	-	-	-	-	-	-
t [nm][r= 1050 g/cc]	207	166	445	426	132	248	150	225
Shear Modulus G [MPa]	-	-	-	-	-	-	-	-

* No data appear for sensors S1-S4 in the Spin Coated section of the table as they were not spin coated. Shear moduli are not given for some of the measurements where the dissipation is too small to use the Voigt model.

porous polymer films can also be measured by alternative methods such as dynamic mechanical analysis (DMA) and buckling techniques.[29-32] Using these alternative methods, the shear moduli for the spin coated and thermally annealed films can be obtained and compared to that of the spray coated films.[33] Further work is needed to determine whether the moduli obtained from DMA and buckling methods are comparable to the *G* obtained at MHz frequency through QCM-D measurements.

In the data labeled *Spray Coated* in Table I, estimated Voigt mass and dissipation values for sensors S1-S4, in which ESD films were applied directly onto the gold, are similar. However, the characteristics of the ESD samples on spin coated PS substrates prepared at similar spray parameters are different. This is obviously due to the differences in the interactions between spray coated PS particles with the gold substrate in one hand and the spin coated PS surface in the other. Additionally, sensors S5-S8, which were spin and spray coated, lack this reproducibility in mass and dissipation. There are also inconsistencies in the material properties obtained from sensors, S5-S6 and S7-S8. These results are likely due to variations in the spray process that result in differences of interfacial adhesion between the spin coated and ESD films. The differences between S5 and S6 is most likely because only a small mass of PS was deposited during the ESD process on S5 compared to that in S8 (Δf increase from 775 to 872 in S5 compared to 738 to 1839 in S8). The difference in *G* values for S7, S8 (2.15 and 1.08 MPa, respectively) could be due to the differences in adhesion between the spin and spray coated layers. The large dissipation in S6-S8, increase by at least an order of magnitude from spin to spray coating, allows the use of the Voigt model.

Dissipation in S1-S4 where PS was sprayed directly onto gold, appear to be directly proportional to flow rate, with increasing flow rate from 0.5 to 1.5 ml/h leading to five-fold increase in dissipation. This is associated with the 3 to 5 times increase in size at these two flow rates. Increase in dissipation with vesicular particles has also been reported in the

literature. It is expected that smaller ESD particles to show smaller dissipation, almost an order of magnitude smaller, compared to the larger particles. Larger particles allow for greater shear displacement under oscillatory motion.[34] The underlying mechanism for an increase in dissipation is likely a result of shear at both the particle-substrate and particle-particle interfaces. These losses are due to friction between these surfaces, and do not appear to depend on particle size (i.e. flow rate) since the Voigt model of viscoelasticity is independent of thickness.[35] In contrast, the shear modulus is observed to be independent of flow rate. The underlying mechanism for an increase in dissipation is likely a result of shear at both the particle-substrate and particle-particle interfaces. This could depend on both the particle size that depends on the flow rate, and the changes in the inter-particle contact due to dissimilarity in particle diameters leading to changes in interstitial pore sizes. In contrast, the shear modulus, the real, or elastic component of the modulus does not change with the particle dimensions.

There is a marked difference in the mass and dissipation values in the two batches of experiments, S1-S4 where PS was sprayed onto gold, and S6-S8 where PS was sprayed on spin coated PS. While the mass on Au at 1.5 ml/h is almost double that at 0.5 ml/h, as is expected since the larger particles at higher flow rates. On spin coated PS, the mass of the electrosprayed PS is about the same at low and high flow rates. One reason is that the mass deposition decreases in highly non-linear fashion because of the charges deposited in the preexisting layers, i.e., on set of self-limiting electrospray.[12] It is also likely that the ESD shells on the spin coated film do not well adhered spin coated PS layer. This mass difference is also reflected in smaller dissipation values when PS is electrosprayed on to spin coated PS.

2.3 Thermal Annealing

Thermal annealing results in an increase in Δf and a decrease in ΔD in all sensors, indicating that the film layer condenses and behaves more elastically as the PS shells collapse and adhere more rigidly to quartz sensor. This increase in film stiffness is apparent in the *Annealing* section

of Table 1. As a result, Voigt model is no longer applicable since the dissipation is negligible as a result of stronger interfacial bonding between the PS film and the quartz crystal sensor. Although the dissipation decreases by a factor of three upon annealing, it is still substantial (Table 1). This is likely due to incomplete collapse of the shells as can be seen in the SEM images (Figure 2f and 2g).

These changes in the QCM-D data upon annealing is corroborated by the work by Keller and Kasemo, who used QCM to study the formation of unilamellar vesicles.[24] The spherical shell-like vesicles illustrated in their work are similar to that of the hollow PS particles shown in Figure 3. While the thinner and more rigidly adhered vesicle monolayers and bilayers observed in Keller and Kasemo's assessment more closely resemble that of the spin coated and annealed films reviewed in this study. Greater dissipation was observed for spherical vesicles, which they ascribed to the structures' ability to undergo larger shear deformation, expressed as a measure of internal friction. Dissipation values for the monolayer and bilayer structures were considered negligible.[24]

Our observations with annealed films are also consistent with the work of Reviakine et al. who reported an increase in Δf and a decrease in ΔD as spherical liposomes collapsed into flat lipid.[36] They used QCM-D to probe the adsorption properties of films consisting of discrete particles with negligible dissipation. Further, they suggested that for layers of laterally heterogenous discrete particles in which dissipation is appreciable, it tends to be dominant at the point of particle-surface contact and the particle-liquid interface.

2.4 Comparison to Bulk Mechanical Properties

Analysis of films produced in the SLED regime typically contain 60-90% porosity, similar to that of extruded polystyrene foams (XPS).[20, 37] Using four-point bending and in-plane shear tests on XPS, Yoshihara and Ataka obtain in-plane shear moduli values between 4.0-9.0 MPa.[37]

While these values are higher than that obtained for the spray coated films in this work (2.03-2.38 MPa), they are surprisingly of similar magnitude. Observable differences may presumably be on account of discrepancies in the underlying polymer and structural properties (*e.g.*, molecular weight and nominal porosity). Strain-rate dependency can also impact these results; while the in-plane shear test might be considered quasi-static, QCM-D is a high-frequency characterization method. Assuming that the sprayed deposited shells are spherical, estimate of the mechanical stiffness of a PS shell can be determined using shell theory.

The shell thickness can be determined using the expression,

$$p = 1 - \left(\frac{V_{shell}}{V_{sphere}} \, v_f \right), \qquad 1$$

Where p is porosity, v_f is volume fraction, V_{shell} is the volume of the shell, and V_{sphere} is the spherical volume. For a mean shell diameter of $3.0 \ \mu m$, v_f=0.65 (consistent with random close packing in each of the principal directions), and p=0.8, the average shell thickness is 154 nm, which is consistent with SEM measurements of ~100 nm at a flow rate 0.5 mL/hr. For thin curved shells, the elastic strain energy, in terms of the 3D elastic modulus E, can be described by considering the deformation of their middle surface, a 2D manifold. Naghdi et al. developed a methodology to reduce the. equations of a solid 3D deformable continuum to those of a thin body by analyzing the manner in which the kinematical vectors (directors) encode the material properties at each material point in the continua.[38] This direct approach reformulates shell theory by modeling a shell as a deformable surface with a single kinematical vector. For a spherical shell, the mechanics is usually associated with its midsurface, a 2D manifold embedded in 3D space. Under these circumstances, a 2D Young's modulus E_{shell} and, bending rigidity κ, can thus be defined as

$$E_{shell} = Eh \qquad 2$$

$$\kappa = \frac{Eh^3}{12(1-\nu^2)}, \quad 3$$

where h is the thickness of the shell and ν is the Poison's ratio. Note that these properties are strongly scale dependent. The validity of the applying shell theory can be determined by computing the Föppl–von Kármán number, which is given by,

$$\gamma = \frac{E_{shell}D^2}{4\kappa}, \quad 4$$

Föppl–von Kármán number, γ is a dimensionless number that quantifies the ratio of the stretching to the bending energy of a shell. It is also a measure of the validity of applying shell theory. γ γis large for thin shells. Typical values of γ for red blood cells (RBC) is of the order of $10^4 \sim 10^5$.[39] Large values of γ thus improves confidence in approximating a 3D shell with a 2D abstraction. Thus, shell theory is relevant when $h \approx 0.1R$ and $\gamma \geq 1000$.[39, 40] Based on the above parameters for spray deposited shells, $h = 85$ nm and $\gamma = 1105$. Bulk PS material is estimated with an average Young's modulus of 3.3 GPa. From Table 1, it is evident that the modulus of spray coated PS is only 0.08-0.20% of the bulk material. The calculated E_{shell} value for a single PS shell is 507 N/m. When comparing the shear modulus (Table 1) with a single shell, the ratio of stiffness of spray coated PS to a single shell is approximately (5.00 - 13.3) x 10^3 m^{-1}. The stiffened response of spray coated PS can be attributed to the shell-shell interactions and shell-surface interactions. To quantify the individual contributions of the different interactions, number of shells within spray coated PS, a number of simulation techniques can be used in future work; *e.g.*, Monte Carlo methods, continuum based microscale homogenization methods and coarse-grained molecular dynamics simulations.[41]

Additionally, the effect of areal density can be inferred from the data spray coated sensors. It is suggested that for a given number of sprays coated layers, as the areal density (number of particles per unit area) increases, the dissipation would seemingly increase; as the

magnitude of particle-particle interactions would increase, leading to energy losses at particle-particle and particle-substrate interfaces.

With regard to thermal annealing and its influence on the mechanical properties of thin shells, it is important to first consider the scale of stress localization. For curved surfaces, the out-of-plane displacements and in-plane strains are strongly coupled. As a result, the normal deformations tend to be localized to narrow widths in shells. The localized deformation length[39] can by computed by

$$l_e = \frac{D}{2\gamma^{\frac{1}{4}}}, \tag{5}$$

For spray coated PS shells, $l_e \approx 260nm$. Given the value of stress localization there is greater tendency for the shells to buckle even at room temperatures. Kosmrlj and Nelson showed using perturbative renormalization group theory via a statistical mechanics approach that for curved shells under thermal fluctuations, the 2D elastic parameters scale inversely to the thermal length, l_{th} such that, $\kappa_R \approx \kappa \left(\frac{l}{l_{th}}\right)^{\eta}$ and $E_{shell_R} \approx E_{shell} \left(\frac{l}{l_{th}}\right)^{-\eta_u}$.[40] Where κ_R and E_{shell_R} are the renormalized parameters, the thermal length l_{th} is the length scale where thermal fluctuations become important for flat membranes, l is the length scale of the shells, η and η_u are constants related by the Ward identity, $\eta_u + \eta = 2$.[40] The thermal length can by determined by

$$l_{th} = \sqrt{\frac{16\pi^3\kappa^2}{3k_B T E_{shell}}}, \tag{6}$$

where k_B is the Boltzmann's constant and T is the temperature. The critical buckling pressure for spherical shells under the classical theory is given by

$$p_{cr} = \frac{\sqrt{(\kappa E_{shell})}}{D^2} \tag{7}$$

Under thermal fluctuations, the critical buckling pressure can be written in terms of the renormalized parameters,

$$p_{cr_R} = \frac{\sqrt{\left(\kappa_R E_{shell_R}\right)}}{D^2} \quad 8$$

For the annealed shells that were heated approximately to the glass transition temperature of 393 K, the ratio of the renormalized critical buckling pressure to the classical pressure is ≈ 0.2. Given the substantial reduction in the magnitude the critical buckling pressure under elevated temperatures, it is safe to postulate that the annealed shells collapse spontaneously due to thermal fluctuations and form a continuous film (Table 1).

Work by Wang and colleagues on modeling viscoelastic contact may indicate that as the number of particles of a given size, all other things held constant, a corresponding of increase in coulombic friction at the particle-particle interfaces would likely increase, leading to more dissipative behavior.[42] However, quantitively decoupling energy dissipation mechanisms in the viscoelastic interactions of discrete particles is beyond the scope of this study and should be explored in future work. This work demonstrates, with further refinement of polymer thin film fabrication and more robust viscoelastic modeling, bulk material properties may be extrapolated from nanogram quantities of polymer materials using QCM-D.

2.5 Limitations of Polymer Film Mechanical Characterization Techniques

Identifying the key deformation mechanisms influencing dissipation in ESD films requires analysis across various spray parameters and loading conditions. Previous studies on the nanoindentation of ESD films (for strain rates ~$10^{-1}s^{-1}$) reveal that the collapse of the polymer shell walls and overall particle network are principal failure modes up to ~20% strain, leading to considerable plastic deformation upon unloading.[5] After this threshold, film densification and viscoelastic behavior in the form of creep become significant. Near ~70% strain, the

substrate's influence dominates, as indicated by a sharp rise in the load vs. depth curve, showcasing the elastic properties of the rigid Si substrate.[5] Similar behavior was noted by Chung et al. upon the nanoindentation of PS films, in which the plastic zone of deformation extended beyond the thickness of the film, resulting in strong interactions between the film and substrate at the interface, leading to overestimation of the indentation modulus by more than order of magnitude.[43] Herbert et al assess experimental methods for probing the viscoelastic behavior of polymers subject to oscillating loads between 0-300 Hz.[44] However, there is a dearth of literature comparing moduli values obtained at low frequencies (10^0-10^3 Hz) to the MHz frequencies encountered in QCM-D. Future work should compare moduli obtained from dynamic nanoindentation of viscoelastic particles subject to harmonic loading to the complex moduli resulting from QCM-D for polymer particles.

In addition, LIPIT has been used to assess the mechanical performance of ESD films subject to high strain rates (10^1-10^6 s^{-1}).[17] The observed dissipation under these conditions was attributed to the collapse of the porous film and thermo-mechanical melting. For some samples under high-speed conditions (>700 m/s), substrate interactions had significant influence on the material and structural behavior of the films, and infrequently led to complete disintegration of the impacting particle.[17] Both LIPIT and nanoindentation exhibit experimental limitations due to nanoparticle confinement at the substrate interface, resulting from the geometric constraints of the impacting particle and indenter tip, respectively. QCM-D facilitates characterization of the complex moduli and dissipative response of polymeric materials yet is not subject to the geometric limitations observed in LIPIT and nanoindentation due to its loading configuration. Thus, QCM-D provides an auxiliary method of mechanical characterization at high strain rates.

ESD was performed under ambient conditions to demonstrate its potential for easy manufacturing of tunable micro/nanoparticles layers. However, variations in ESD processing, especially when applied to the spin coat PS films, can lead to a lack of uniformity at the coating

interface. Future work could mitigate this by controlling environmental conditions during ESD, such as substrate-temperature, humidity, and the electrostatic "charge landscape," similar to what has been conducted in recent demonstrations in ESD for bioactive coatings[45] and sub-micron deposition. Further research is necessary to accurately model the mechanical behavior of such films, particularly for applications involving protein adsorption onto ESD films.[46]

3. Conclusions

In this work, QCM-D was used for the first time to analyze viscoelastic behavior of polymer shells of varying sizes produced by ESD and subject to MHz range shear oscillations. ESD films deposited directly onto bare quartz sensors exhibit larger shifts in dissipation compared to sprayed films deposited onto smooth PS films for all flow rates. Films electrosprayed at 1.5 mL/h showed two times the Δf and an order of magnitude increases in ΔD compared to the films deposited at 0.5 mL/h. The larger shifts in Δf and ΔD are caused by larger particle diameters produced at higher flow rates, attributed to a higher degree of shear deformation and internal friction. Films produced a 0.5 mL/h behaved more elastically, owing to a shorter in interparticle distance and an increase in interparticle fusion due to localized region of unevaporated solvent. Data obtained from Voigt model analysis reveal that, the shear moduli of ESD films are flow rate independent within experimental error. Sauerbrey model was used to estimate the properties of the spin coat and thermally annealed PS coatings. Further work is needed to develop more robust mechanical models for complex multilayer films that can account for the behavior of multilayers discrete particles exhibiting viscoelastic behavior. A comparison of the observed mechanical characteristics on shells at high frequencies to the static bulk properties show that the observed modulus is 0.002 times the bulk modulus but is 5-10 thousand times stiffer than a single shell because interfacial interactions between the shells and the substrate. As far as we know, this is the first report of the shear behavior of polystyrene nanoshells that focuses on interparticle friction.

Unlike LIPIT and nanoindentation, QCM-D offers the ability to evaluate the viscoelastic properties of ESD films without the limitations of size dependent artifacts arising from the impacting particle or indenter tip, respectively. Additionally, confinement effects often seen in mechanical characterization of nanoparticles on rigid substrates, appears to be negligible for QCM-D; resulting from shear induced deformation as opposed to a loading condition normal to the surface of the film, as is the case in atomic force microscopy (AFM), LIPIT, and nanoindenation.[47, 48]

Future work can look to develop models of coupled storage and loss elements comparable to dynamic mechanical analysis (DMA). Applications of ESD and QCM-D in tandem could serve as a novel method for facile fabrication and evaluation of polymer separators, solid polyelectrolytes, or hybrid polymer electrodes for use in solid state batteries. Further, a parametric study is recommended to optimize film deposition techniques so QCM-D can be used to develop ESD sensors with tunable size selectivity for nanogram quantities of gases, liquids, or bioactive particles.

4. Experimental Section

Sample Fabrication:

The results from one of the five experiments are being reported here. The five experiments were carried out with small changes in the electrospraying protocol to improve the quality of the deposition. The results from all the experiments were similar, demonstrating the reproducibility of the fabrication and measurement procedures. ESD was used to deposit polystyrene (PS) [molecular weight (MW) = 35 kDa] (Millipore Sigma, USA) shells onto gold plated quartz crystal sensors as described in previous work.[5] A 1 wt.% solution of PS in 2-butanone (MEK) (Millipore Sigma, USA) was chosen due to produce tunable nano/microscale particles. ESD parameters were selected to ensure stability of the Taylor cone, and to produce microscale PS particles of varying sizes.[5, 49] During the spray process, each quartz crystal was adhered to a 100 cm p-type boron doped silicon wafer [0-100 Ω-cm] (University Wafer, USA) using a drop of deionized water to improve the interfacial contact between the bottom of the sensor and the top of the wafer. The wafer was then mounted on an aluminum plate and electrically grounded. The substrates were sprayed at ambient conditions (~20°C) and 20-50% relative humidity. The ability to spray this solution in ambient humidity is ostensibly enabled by the hydrophobic nature of the phenyl and methyl functional groups of the PS and MEK, respectively.[50, 51] The nozzle and extractor ring distances and voltages were 4 and 5 cm, and 6 and 4 kV, respectively.

SEM Characterization:

Si wafer chips (1 cm x 1 cm) were sprayed with PS at the given spray parameters in ambient conditions. Gold sputtering was used to deposit 10 nm of Au onto the PS particles. SEM images were taken with a 5kV driving voltage in a Zeiss Sigma FESEM with EBSD (Zeiss, Germany), and the microstructure is observed.

QCMD Experimental Procedures:

QCM-D measurements were carried out on a QSense Pro instrument (Biolin Scientific, Sweden). Bare Au-plated quartz crystals were first measured to establish a baseline frequency and dissipation prior to sequential spin coating, electrospraying, and finally, thermal annealing. Sensors 1-8 (S1-S8) were prepared as follows: S5-S8 were spin coated with a 5% MEK solution of PS at 2000 RPM for 30 s to presumably provide improved interfacial contact with the ESD films, initially thought to be enhanced by solvent vapor swelling. S1, S2, S5, and S6 were sprayed at 0.5 mL/h for 18 minutes, while S3, S4, S7, and S8 were all sprayed at 1.5 mL/h for 6 minutes. All samples were sprayed with 0.15 mL of 1 wt.% PS solution to ensure uniform mass deposition, but at different flow rates to achieve PS particles of varying sizes.

Thermal Annealing:

After obtaining QCM-D data from the spray-coated samples, all samples were thermally annealed on a hotplate at 120°C (above the T_g of PS) for ~10 minutes to smooth the particles into a continuous film. Frequency and dissipation data were obtained on these smoothed thin films.

QCMD Data Analysis:

Frequency and dissipation data from all the steps were stitched together and analyzed using QTools analysis software. QCM-D data are typically presented as the changes in the frequency of oscillation of the quartz sensor crystal (Δf), and the changes in ΔD.[18, 19, 52] It is important to note that the frequency and dissipation data from separate measurements done on different day are presented as one continuous scan, even though it is not, using a tool called stitching in the QTools analysis software.

If ΔD (which reflects the time-dependent properties of the deposited layers) is small, then Δf can be used determine the adsorbed mass (Δm). A decrease in frequency indicates

adsorption of mass, and conversely an increase indicates mass loss, as given by the Sauerbrey equation:

$$\Delta m = -\left(\frac{C}{n}\right)\Delta f \quad (1)$$

where C is the mass sensitivity constant (17.7 ng/cm^2), and n is the overtone number (1, 3, …,13).[52] ΔD was small in many instances, <0.3*10^{-6} units of ΔD per 10 Hz Δf. It is generally understood that Sauerbrey equation can be used when ΔD is < 0.5*10^{-6} 10 Hz of Δf ;this is higher than the commonly accepted threshold proposed by Reviakine et al., $\left|\frac{\Delta D}{\Delta f_n}\right| <$ 4 x 10^{-7} Hz^{-1}, for applying the Sauerbrey equation.[36, 53]. Voigt viscoelastic model does not work when the dissipations are this small. When the dissipation was significant, it was between 1 and 2 x 10^{-6} units per 10 Hz of Δf , the Voigt model was used to analyze the data and obtain the adsorbed thickness (assuming an effective density of 1050 kg cm^{-3}) and shear modulus of the electrosprayed layer.[52] These values, reported in Table 1, were obtained using QTools software provided by the manufacturer of the instrument. Although the Sauerbrey equation and Voigt models are strictly applicable to uniform films, it has been shown these can be used even with monolayers of discrete particles or other nanosized objects.[34, 36]

Supporting Information

A PDF of the raw and fitted QCMD data plots are available in the Wiley Online Library or from the author.

Acknowledgements

This work was partially funded by the NSF through CMMI Award 2019849. R.A.G.-W. acknowledges support from the National GEM Consortium and the US Department of Defense SMART Scholarship Program. N.M.M. acknowledges support from the New Jersey Space Grant Consortium, funded by NASA, through the student fellow program.

Conflict of Interest Statement

J.P.S. is coinventor of three patents/applications on self-limiting electrospray deposition. Otherwise, the Authors have no conflict of interest relevant to this article.

N. Sanjeeva Murthy

ORCID: 0000-0002-2324-5874

Jonathan. P. Singer

ORCID: 0000-0002-5934-8795

Robert A. Green-Warren

ORCID: 0000-0002-3842-2140

Assimina A. Pelegri

ORCID: 0000-0003-1145-8175

Received: ((will be filled in by the editorial staff))

Revised: ((will be filled in by the editorial staff))

Published online: ((will be filled in by the editorial staff))

References

(1) Hołda, A. K.; Vankelecom, I. F. J. Understanding and guiding the phase inversion process for synthesis of solvent resistant nanofiltration membranes. *Journal of Applied Polymer Science* **2015**, *132* (27). DOI: https://doi.org/10.1002/app.42130.
(2) Toolan, D. T. W.; Haq, E. u.; Dunbar, A.; Ebbens, S.; Clarke, N.; Topham, P. D.; Howse, J. R. Direct observation of morphological development during the spin-coating of polystyrene–poly(methyl methacrylate) polymer blends. *Journal of Polymer Science Part B: Polymer Physics* **2013**, *51* (11), 875-881. DOI: https://doi.org/10.1002/polb.23288.
(3) Taylor, G. I. Disintegration of water drops in an electric field. *Proceedings of the Royal Society of London. Series A. Mathematical and Physical Sciences* **1964**, *280* (1382), 383-397. DOI: doi:10.1098/rspa.1964.0151.
(4) Lei, L.; Kovacevich, D. A.; Nitzsche, M. P.; Ryu, J.; Al-Marzoki, K.; Rodriguez, G.; Klein, L. C.; Jitianu, A.; Singer, J. P. Obtaining Thickness-Limited Electrospray Deposition for 3D Coating. *ACS Applied Materials & Interfaces* **2018**, *10* (13), 11175-11188. DOI: 10.1021/acsami.7b19812.
(5) Green-Warren, R. A.; Bontoux, L.; McAllister, N. M.; Kovacevich, D. A.; Shaikh, A.; Kuznetsova, C.; Tenorio, M.; Lei, L.; Pelegri, A. A.; Singer, J. P. Determining the Self-Limiting Electrospray Deposition Compositional Limits for Mechanically Tunable Polymer Composites. *ACS Applied Polymer Materials* **2022**, *4* (5), 3511-3519. DOI: 10.1021/acsapm.2c00106.
(6) Kovacevich, D. A.; Lei, L.; Han, D.; Kuznetsova, C.; Kooi, S. E.; Lee, H.; Singer, J. P. Self-Limiting Electrospray Deposition for the Surface Modification of Additively Manufactured Parts. *ACS Applied Materials & Interfaces* **2020**, *12* (18), 20901-20911. DOI: 10.1021/acsami.9b23544.
(7) Kingsley, B. J.; Chiarot, P. R. Polyimide Films Manufactured Using Partially Wet Electrospray Deposition. *ACS Applied Polymer Materials* **2023**, *5* (3), 1797-1809. DOI: 10.1021/acsapm.2c01891.
(8) Tang, J.; Gomez, A. Controlled mesoporous film formation from the deposition of electrosprayed nanoparticles. *Aerosol Science and Technology* **2017**, *51* (6), 755-765. DOI: 10.1080/02786826.2017.1303573.
(9) Kim, J. Y.; Hong, J. G. Effect of Electrical Conductivity on Atomization Characteristics of Electrospray. *Journal of Applied Fluid Mechanics* **2022**, *15* (5), 1427-1436. DOI: 10.47176/jafm.15.05.1094.
(10) Lei, L.; Chen, S.; Nachtigal, C. J.; Moy, T. F.; Yong, X.; Singer, J. P. Homogeneous gelation leads to nanowire forests in the transition between electrospray and electrospinning. *Materials Horizons* **2020**, *7* (10), 2643-2650, 10.1039/D0MH00872A. DOI: 10.1039/D0MH00872A.
(11) Jang, I. R.; Jung, S. I.; Park, J.; Ryu, C.; Park, I.; Kim, S. B.; Kim, H. J. Direct and controlled device integration of graphene oxide on Quartz Crystal Microbalance via electrospray deposition for stable humidity sensing. *Ceramics International* **2022**, *48* (6), 8004-8011. DOI: https://doi.org/10.1016/j.ceramint.2021.11.347.
(12) Lei, L.; Gamboa, A. R.; Kuznetsova, C.; Littlecreek, S.; Wang, J.; Zou, Q.; Zahn, J. D.; Singer, J. P. Self-limiting electrospray deposition on polymer templates. *Scientific Reports* **2020**, *10* (1), 17290. DOI: 10.1038/s41598-020-74146-1.
(13) Brown, N. A.; Zhu, Y.; German, G. K.; Yong, X.; Chiarot, P. R. Electrospray deposit structure of nanoparticle suspensions. *Journal of Electrostatics* **2017**, *90*, 67-73. DOI: https://doi.org/10.1016/j.elstat.2017.09.004.
(14) Blisko, J. M.; Grzenda, M. J.; Vladimirsky, R. M.; Shuck, C. E.; Singer, J. P.; Yong, X. Controlling morphology in electrosprayed methylcellulose nanowires via nanoparticle

addition: coarse-grained modeling and experiments. *Nanoscale* **2022**, *14* (48), 17985-17994, 10.1039/D2NR04177D. DOI: 10.1039/D2NR04177D.
(15) Morais AÍ, S.; Vieira, E. G.; Afewerki, S.; Sousa, R. B.; Honorio, L. M. C.; Cambrussi, A.; Santos, J. A.; Bezerra, R. D. S.; Furtini, J. A. O.; Silva-Filho, E. C.; et al. Fabrication of Polymeric Microparticles by Electrospray: The Impact of Experimental Parameters. *J Funct Biomater* **2020**, *11* (1). DOI: 10.3390/jfb11010004 From NLM.
(16) Lee, J.-H.; Veysset, D.; Singer, J. P.; Retsch, M.; Saini, G.; Pezeril, T.; Nelson, K. A.; Thomas, E. L. High strain rate deformation of layered nanocomposites. *Nature Communications* **2012**, *3* (1), 1164. DOI: 10.1038/ncomms2166.
(17) Ren, Z.; Green-Warren, R.; McAllister, N.; Kim, A.; Shaikh, A.; Pelegri, A. A.; Singer, J. P.; Lee, J.-H. Enhanced mechanical energy absorption via localized viscoplasticity of nano-cellular polymer coating under supersonic impact loading. *Giant* **2023**, *15*, 100180. DOI: https://doi.org/10.1016/j.giant.2023.100180.
(18) Dixon, M. C. Quartz crystal microbalance with dissipation monitoring: enabling real-time characterization of biological materials and their interactions. *J Biomol Tech* **2008**, *19* (3), 151-158. From NLM.
(19) Tarnapolsky, A.; Freger, V. Modeling QCM-D Response to Deposition and Attachment of Microparticles and Living Cells. *Analytical Chemistry* **2018**, *90* (23), 13960-13968. DOI: 10.1021/acs.analchem.8b03411.
(20) McAllister, N.; Green-Warren, R.; Arkhipov, M.; Lee, J.-H.; Pelegri, A.; Singer, J. *Non-Destructive Measurement of Optically Scattering Polymer Films Using Image Processing*; 2023. DOI: 10.26434/chemrxiv-2023-88szt.
(21) Green-Warren, R. M., Noah;Arkhipov, Maxim;Singer, Jonathan. Effects of Solvent Conductivity on the Self-Limiting Electrospray Deposition (SLED) of Polymer Films. In *APS March Meeting 2023*, Bulletin of the American Physical Society, March 2023, 2023; American Physical Society.
(22) Gañán-Calvo, A. M.; Dávila, J.; Barrero, A. Current and droplet size in the electrospraying of liquids. Scaling laws. *Journal of Aerosol Science* **1997**, *28* (2), 249-275, Article. DOI: 10.1016/S0021-8502(96)00433-8 Scopus.
(23) Patel, A.; Lima, M. R. N.; Cho, H.-Y.; Lee, K.-B.; Murthy, N. S.; Kohn, J. Disassembly of Nanospheres with a PEG Shell upon Adsorption onto PEGylated Substrates. *Langmuir* **2020**, *36* (1), 232-241. DOI: 10.1021/acs.langmuir.9b03042.
(24) Keller, C. A.; Kasemo, B. Surface Specific Kinetics of Lipid Vesicle Adsorption Measured with a Quartz Crystal Microbalance. *Biophysical Journal* **1998**, *75* (3), 1397-1402. DOI: 10.1016/S0006-3495(98)74057-3 (acccessed 2024/01/25).
(25) Easley, A. D.; Ma, T.; Eneh, C. I.; Yun, J.; Thakur, R. M.; Lutkenhaus, J. L. A practical guide to quartz crystal microbalance with dissipation monitoring of thin polymer films. *Journal of Polymer Science* **2022**, *60* (7), 1090-1107, https://doi.org/10.1002/pol.20210324. DOI: https://doi.org/10.1002/pol.20210324 (acccessed 2023/05/09).
(26) Alexander, T. E.; Lozeau, L. D.; Camesano, T. A. QCM-D characterization of time-dependence of bacterial adhesion. *The Cell Surface* **2019**, *5*, 100024. DOI: https://doi.org/10.1016/j.tcsw.2019.100024.
(27) Irwin, E. F.; Ho, J. E.; Kane, S. R.; Healy, K. E. Analysis of Interpenetrating Polymer Networks via Quartz Crystal Microbalance with Dissipation Monitoring. *Langmuir* **2005**, *21* (12), 5529-5536. DOI: 10.1021/la0470737.
(28) Johannsmann, D.; Langhoff, A.; Leppin, C. Studying Soft Interfaces with Shear Waves: Principles and Applications of the Quartz Crystal Microbalance (QCM). *Sensors* **2021**, *21*, 3490. DOI: 10.3390/s21103490.

(29) Huang, C. K.; Lou, W. M.; Tsai, C. J.; Wu, T.-C.; Lin, H.-Y. Mechanical properties of polymer thin film measured by the bulge test. *Thin Solid Films* **2007**, *515* (18), 7222-7226. DOI: https://doi.org/10.1016/j.tsf.2007.01.058.
(30) Stafford, C. M.; Harrison, C.; Beers, K. L.; Karim, A.; Amis, E. J.; VanLandingham, M. R.; Kim, H.-C.; Volksen, W.; Miller, R. D.; Simonyi, E. E. A buckling-based metrology for measuring the elastic moduli of polymeric thin films. *Nature Materials* **2004**, *3* (8), 545-550. DOI: 10.1038/nmat1175.
(31) Akabori, K.-i.; Tanaka, K.; Nagamura, T.; Takahara, A.; Kajiyama, T. Molecular Motion in Ultrathin Polystyrene Films: Dynamic Mechanical Analysis of Surface and Interfacial Effects. *Macromolecules* **2005**, *38* (23), 9735-9741. DOI: 10.1021/ma051143e.
(32) Paleti, S. H. K.; Kim, Y.; Kimpel, J.; Craighero, M.; Haraguchi, S.; Müller, C. Impact of doping on the mechanical properties of conjugated polymers. *Chemical Society Reviews* **2024**, *53* (4), 1702-1729, 10.1039/D3CS00833A. DOI: 10.1039/D3CS00833A.
(33) Fu, W.-E.; Chang, Y.-Q.; He, B.-C.; Wu, C.-L. Determination of Young's modulus and Poisson's ratio of thin films by X-ray methods. *Thin Solid Films* **2013**, *544*, 201-205. DOI: https://doi.org/10.1016/j.tsf.2013.03.121.
(34) Reviakine, I.; Rossetti, F.; Morozov, A.; Textor, M. Investigating the properties of supported vesicular layers on titanium dioxide by quartz crystal microbalance with dissipation measurements. *The Journal of chemical physics* **2005**, *122*, 204711. DOI: 10.1063/1.1908500.
(35) Lucklum, R.; Hauptmann, P. The Δf–ΔR QCM technique: an approach to an advanced sensor signal interpretation. *Electrochimica Acta* **2000**, *45* (22), 3907-3916. DOI: https://doi.org/10.1016/S0013-4686(00)00451-5.
(36) Reviakine, I.; Johannsmann, D.; Richter, R. P. Hearing What You Cannot See and Visualizing What You Hear: Interpreting Quartz Crystal Microbalance Data from Solvated Interfaces. *Analytical Chemistry* **2011**, *83* (23), 8838-8848. DOI: 10.1021/ac201778h.
(37) Yoshihara, H.; Ataka, N.; Maruta, M. Measurement of the Young's modulus and shear modulus of extruded polystyrene foam by the longitudinal and flexural vibration methods. *Journal of Cellular Plastics* **2018**, *54* (2), 199-216. DOI: 10.1177/0021955x16681447.
(38) Naghdi, P. M. The Theory of Shells and Plates. 1973; Springer Berlin Heidelberg: pp 425-640.
(39) Paulose, J.; Nelson, D. R. Buckling pathways in spherical shells with soft spots. *Soft Matter* **2013**, *9* (34), 8227-8245, 10.1039/C3SM50719J. DOI: 10.1039/C3SM50719J.
(40) Košmrlj, A.; Nelson, D. R. Statistical Mechanics of Thin Spherical Shells. *Physical Review X* **2017**, *7* (1), 011002. DOI: 10.1103/PhysRevX.7.011002.
(41) Zeng, Q. H.; Yu, A. B.; Lu, G. Q. Multiscale modeling and simulation of polymer nanocomposites. *Progress in Polymer Science* **2008**, *33* (2), 191-269. DOI: https://doi.org/10.1016/j.progpolymsci.2007.09.002.
(42) Wang, D.; de Boer, G.; Neville, A.; Ghanbarzadeh, A. A Review on Modelling of Viscoelastic Contact Problems. *Lubricants* **2022**, *10* (12), 358.
(43) Chung, P. C.; Glynos, E.; Green, P. F. The Elastic Mechanical Response of Supported Thin Polymer Films. *Langmuir* **2014**, *30* (50), 15200-15205. DOI: 10.1021/la503879v.
(44) Herbert, E. G.; Sudharshan Phani, P.; Johanns, K. E. Nanoindentation of viscoelastic solids: A critical assessment of experimental methods. *Current Opinion in Solid State and Materials Science* **2015**, *19* (6), 334-339. DOI: https://doi.org/10.1016/j.cossms.2014.12.006.
(45) Park, S. H.; Lei, L.; D'Souza, D.; Zipkin, R.; DiMartini, E. T.; Atzampou, M.; Lallow, E. O.; Shan, J. W.; Zahn, J. D.; Shreiber, D. I.; et al. Efficient electrospray deposition of surfaces smaller than the spray plume. *Nature Communications* **2023**, *14* (1), 4896. DOI: 10.1038/s41467-023-40638-7.

(46) Rouf, A.; Park, S. H.; Singer, J. P. Sub-Micron Thickness Self-Limiting Electrospray Deposition via Voltage Bias of Spray Target. *Advanced Materials Interfaces n/a* (n/a), 2300982. DOI: https://doi.org/10.1002/admi.202300982.
(47) Wang, H.; Qiang, Y.; Shamsabadi, A. A.; Mazumder, P.; Turner, K. T.; Lee, D.; Fakhraai, Z. Thermal Degradation of Polystyrene under Extreme Nanoconfinement. *ACS Macro Letters* **2019**, *8* (11), 1413-1418. DOI: 10.1021/acsmacrolett.9b00649.
(48) Song, J.; Kahraman, R.; Collinson, D. W.; Xia, W.; Brinson, L. C.; Keten, S. Temperature effects on the nanoindentation characterization of stiffness gradients in confined polymers. *Soft Matter* **2019**, *15* (3), 359-370, 10.1039/C8SM01539B. DOI: 10.1039/C8SM01539B.
(49) Sneddon, I. N. The relation between load and penetration in the axisymmetric boussinesq problem for a punch of arbitrary profile. *International Journal of Engineering Science* **1965**, *3* (1), 47-57. DOI: https://doi.org/10.1016/0020-7225(65)90019-4.
(50) Barchi, J. J., Jr.; Strain, C. N. The effect of a methyl group on structure and function: Serine vs. threonine glycosylation and phosphorylation. *Front Mol Biosci* **2023**, *10*, 1117850. DOI: 10.3389/fmolb.2023.1117850 From NLM.
(51) Kim, J. M.; Lin, Y.-H.; Aravindhan, P. P.; Beckingham, B. S. Impact of hydrophobic pendant phenyl groups on transport and co-transport of methanol and acetate in PEGDA-SPMAK cation exchange membranes. *Chemical Engineering Research and Design* **2022**, *185*, 418-429. DOI: https://doi.org/10.1016/j.cherd.2022.07.017.
(52) Höök, F.; Kasemo, B.; Nylander, T.; Fant, C.; Sott, K.; Elwing, H. Variations in Coupled Water, Viscoelastic Properties, and Film Thickness of a Mefp-1 Protein Film during Adsorption and Cross-Linking: A Quartz Crystal Microbalance with Dissipation Monitoring, Ellipsometry, and Surface Plasmon Resonance Study. *Analytical Chemistry* **2001**, *73* (24), 5796-5804. DOI: 10.1021/ac0106501.
(53) Sadman, K.; Wiener, C. G.; Weiss, R. A.; White, C. C.; Shull, K. R.; Vogt, B. D. Quantitative Rheometry of Thin Soft Materials Using the Quartz Crystal Microbalance with Dissipation. *Analytical Chemistry* **2018**, *90* (6), 4079-4088. DOI: 10.1021/acs.analchem.7b05423.